PSFC/JA-07-4

H-Mode Pedestal and Threshold Studies Over an Expanded Operating Space on Alcator C-Mod

A.E. Hubbard, J.W. Hughes, I.O. Bespamyatnov*, T. Biewer**, I. Cziegler, B. LaBombard, Y. Lin, R. McDermott, J.E. Rice, W.L. Rowan*, J.A. Snipes, J.L. Terry, S.M. Wolfe, S. Wukitch and the Alcator C-Mod Group

* Fusion Research Center, Univ. Texas at Austin, Austin, TX 78712
**Oak Ridge National Lab, PO Box 2008, Oak Ridge, TN 37831

April 2007

Plasma Science and Fusion Center
Massachusetts Institute of Technology
Cambridge MA 02139 USA

This work was supported by the U.S. Department of Energy, Grant DE DE-FC02-99ER54512. Reproduction, translation, publication, use and disposal, in whole or in part, by or for the United States government is permitted.

Submitted for publication to *Physics of Plasmas.*

H-mode pedestal and threshold studies over an expanded operating space on Alcator C-Mod

A. E. Hubbard, J. W. Hughes, I. O. Bespamyatnov*, T. Biewer[#], I. Cziegler, B. LaBombard, Y. Lin, R. McDermott, J. E. Rice, W. L. Rowan*, J. A. Snipes, J. L. Terry, S. M. Wolfe, S. Wukitch and the Alcator C-Mod Group

Plasma Science and Fusion Center, MIT, Cambridge, MA 02129

*Fusion Research Center, Univ. Texas at Austin, Austin, TX 78712

[#] Oak Ridge National Lab, PO Box 2008, Oak Ridge, TN 37831 USA

ABSTRACT

This paper reports on studies of the edge transport barrier and transition threshold of the High Confinement (H) mode of operation on the Alcator C-Mod tokamak [I. H. Hutchinson *et al*, Phys. Plasmas **1**, 1511 (1994)], over a wide range of toroidal field (2.6-7.86 T) and plasma current (0.4-1.7 MA). The H-mode power threshold and edge temperature at the transition increase with field. Barrier widths, pressure limits and confinement are nearly independent of field at constant current, but the operational space at high B shifts towards higher temperature and lower density and collisionality. Experiments with reversed field and current show that scrape-off-layer flows in the high field side depend primarily on configuration. In configurations with the B×∇B drift away from the active X-point, these flows lead to more counter-current core rotation which apparently contributes to higher H-mode thresholds. In the unfavorable case, edge temperature thresholds are higher and slow evolution of profiles indicates a reduction in thermal transport prior to the transition in particle confinement. Pedestal temperatures in this case are also higher than in the favorable configuration. Both high field and reversed field results suggest that parameters at the L-H transition are influencing the evolution and parameters of the H-mode pedestal.

I. Introduction and Background

This paper reports on results obtained in recent H-mode experiments on the compact, high field, Alcator C-Mod tokamak[1] over extended operational parameters, in particular higher magnetic field B_T, up to 7.85 T, and unfavorable B×∇B drift direction. The high confinement, or "H-

mode" regime, first observed on ASDEX[2], is characterized by a steepening of edge temperature and density gradients due to reduced transport - the so-called edge "pedestal". This in turn, through stiffness in the temperature profile[3] and generally flat density profiles, leads to increases in total stored energy W and global energy confinement time τ_E; W is well correlated on C-mod as several other experiments with the pedestal pressure $p_{e,ped}$[4]. H-modes have now been observed on C-Mod for over ten years[5], and studied with an increasingly detailed array of high resolution diagnostics, as recently reviewed[6]. H-mode regimes on C-Mod are somewhat different than on most other tokamaks. Most common, and most extensively studied, are the edge localized mode (ELM)-free regime, which has low particle transport and leads to transient H-modes with ramping electron density n_e and radiated power P_{rad}, and the Enhanced D-alpha (EDA) regime. The latter is characterized by a continuous edge 'quasicoherent' (QC) mode, which increases effective edge particle diffusivity, D_{eff} and enables long, steady H-modes with constant n_e and lower P_{rad}[7]. This regime is favored by higher safety factor, q_{95}, and pedestal collisionality, ν^*_{ped}, and occurs at moderate edge pressure, with normalized pressure gradient α_{MHD} below the peeling-ballooning stability limit[8]. When α_{MHD} is increased, the QC mode weakens or broadens, and small, irregular ELMs are seen. This regime is likely related to Type II or grassy ELMs seen on other devices, as recently reviewed[9]. A regime of larger, discrete ELMs has recently been observed with strong shaping and low ν^*_{ped}[10,11].

Alcator C-Mod relies exclusively on RF heating, primarily ion cyclotron resonance heating (ICRH), with 8 MW of source power. For near-central heating, the B_T is thus restricted by the ICRH frequency and scenario. Half of the source power is fixed at 80 MHz, while the remaining 4 MW is tunable from 50-80 MHz. Most prior H-mode threshold and pedestal studies have been done at B_T~5.4 T, with D(H) minority heating at 78-80 MHz, with extension in 2005 down to 2.6 T using 2nd harmonic heating, and at I_p range 0.4-1.5 MA. To summarize these results, n_e and T_e pedestal widths measured using high resolution Edge Thomson Scattering (ETS)[12] are extremely narrow, typically 2-5 mm, and generally do not show systematic scalings with B_T, I_p, or pedestal density, n_{ped}[13,14], in contrast to some results elsewhere[15,16]. There are some exceptions to this rule. In particular the density pedestal becomes wider at very low (for C-Mod) n_{ped} (~$10^{20}m^{-3}$)

and I_p (~400 kA) or with strong shaping. Under normal operation, though, widths are fixed, and pedestal heights are dominated by scalings of the gradients in n_e, T_e and p_e. These, in turn, appear to depend on transport in the barrier region. In EDA H-modes, pedestal α_{MHD} is restricted to a band which increases at lower ν^*_{ped}[14], suggesting a possible connection to critical-gradient models as in the scrape-off layer (SOL)[17]. Analysis of the density sources and pedestal shows that, at the higher densities of most C-Mod operation, ionization is primarily in the SOL, and also that a particle diffusivity "well" exists in the pedestal region, with decreasing D_{eff} at higher I_p[14]. n_{ped} thus scales strongly with I_p, with a weaker dependence on the density of the target plasma, ~ $n_{e,L}^{0.4}$. Gas fuelling efficiency into an established H-mode is very low, particularly at high I_p[18,19]. Understanding the intrinsic scaling of the density pedestal is thus key to predicting the accessible pedestal parameters and need for other fuelling methods on future experiments such as ITER.

High power thresholds at the maximum C-Mod B_T of 8 T, coupled with the need to use D(He^3) ICRH, which has lower single-pass absorption, make H-mode experiments challenging; a few short-lived 8 T H-modes were produced in early C-Mod operation which confirmed high L-H power thresholds[20], but few high-resolution diagnostics were then available. Recent experiments to optimize D(He^3) heating succeeded in demonstrating efficiencies and confinement comparable to D(H) heating. New experimental results on H-mode pedestals and thresholds including B_T and I_p up to 7.85 T and 1.7 MA, as summarized in the operational space plot shown in Figure 1, are reported in Section II. These reveal in particular some differences in density pedestal scaling, and lower collisionality at higher field.

The transition from L-mode to H-mode has also been studied extensively on Alcator C-Mod[6]. Early experiments showed, for given I_p, B_T and magnetic configuration, a local threshold condition in edge T_e or a closely related parameter[20]. It was noted that this 'threshold T_e' increased with B_T, and was about a factor of two higher for plasmas with unfavorable magnetic configuration, i.e. with $B\times\nabla B$ drifts away from the active X-point, though the reason for the latter was unclear. Consistent results were also found on other tokamaks[21,22]. Recent SOL flow

measurements have provided insight into a possible reason for the configuration dependence on the threshold. Strong parallel flows are observed along field lines to the active divertor[23,24]. These flows, apparently driven by ballooning-like transport fluxes, are highest at the high-field side (HFS), reaching near-sonic speeds. HFS flows reverse direction when the configuration is changed from lower single null (LSN) to upper null (USN) and are small in double null. Interestingly, these flows correlate well with core toroidal rotation $V_{tor}(0)$ in ohmic L-modes, apparently providing a variable boundary condition. It should be noted that all C-Mod plasmas are free of external torque. Intrinsic core flows also have other components, which are complex and poorly understood; V_{tor} tends to increment in a co-I_p direction when plasma pressure increases[25]. Interestingly, $V_{tor}(0)$ was at about the same value at the L-H transition in all three configurations in the 5.4 T, 0.8 MA discharges studied, suggesting that a parameter related to the rotation is important for the transition and that the difference in edge flows may be responsible for the differences in threshold, though not necessarily for the L-H transition itself[24].

Comparisons of different configurations leave some ambiguities, since upper and lower divertor geometries on C-Mod are quite different. New experiments have been conducted which compare flows and L-H thresholds in the same configuration, with fields and currents reversed. These results are presented in Section III. Evolution of edge thermal transport before the transitions in the unfavorable case, similar in several respects to observations on ASDEX Upgrade[22] is discussed. Comparisons of pedestal parameters also reveal some differences with field direction. These and other implications of the expanded C-Mod results, including apparent connections between threshold and pedestal parameters, are discussed in Section IV.

II H-mode experiments including high magnetic field

A. L-H threshold

As expected, the H-mode power threshold rises with B_T. Figure 2 compares total power P_{thresh} (P_{RF} +P_{ohmic}, assuming 80% RF absorption efficiency) at the L-H transition (a) and T_e at the 95% flux surface (b, measured at nearest preceding ETS profile) for discharges at 5.4 T and 7.85 T. P_{thresh} is typically 2.7-4 MW at B_T=7.85 T, with a few cases as high as 5 MW at I_p=1.7 MA, though the I_p dependence has not been systematically explored. Prior global scalings of P_{thresh},

mainly at lower field, include $P_{thresh}=1.42\ n_e^{0.58}\ B_T^{0.82}\ R^{1.0}\ a^{0.81}$, from multi-machine scalings including C-Mod data, and $P_{thresh}=1.49\ n_e^{0.59}\ B_T^{1.05}\ R^{0.75}\ a^{0.84}$ from C-Mod data alone[26]. The new 8 T data suggest an even stronger dependence on B_T. However, possible differences in RF absorption in the two heating scenarios could affect the coefficient, and more study would be needed before modifying scaling expressions. Edge T, and ∇T, are also significantly increased at the higher B_T. Transition temperature is correlated with P_{thresh}/n_e, as shown in Figure 2(c), indicating approximately constant edge transport. It should be noted that these were not carefully controlled threshold experiments with power slowly ramped or stepped in small increments, which accounts for the larger scatter than in prior studies[20]. However, the general trend is clear; edge T_e at the high-B transition, up to 400 eV, is comparable to H-mode T_{ped} in many lower B discharges. This initial condition very likely affects the subsequent n-T trajectory of the following H-mode.

B. Pedestal parameter scaling

Electron pedestal parameters have been determined for a large dataset of H-mode discharges at near-constant shape, now over an expanded range $0.4 \leq I_p \leq 1.7$ MA and $2.6 < B_T \leq 7.85$ T. Pedestal heights and widths are determined using a fit to a modified tanh function[13]. All pedestal widths continue to be largely invariant with I_p and B_T despite the factor of 4 and 3 ranges respectively, essentially ruling out a simple functional dependence on ρ_{pol} or ρ_{tor}. The dataset also spans a wide range of collisionality at the pedestal, ν^*_{ped} =0.44-12, defined as the ratio of the collision frequency to the bounce frequency, $\nu_e^* = 6.921\times10^{18}\, q_{95} R n_e Z_{eff} \ln\Lambda / (T_e^2\, \varepsilon^{3/2})$. There is little evident dependence of widths on ν^*_{ped}. As noted above, the exception seems to be wider pedestals at the lowest I_p and n_{ped}. The most apparent difference in high B discharges is in the pedestal density. The new 7.85 T data fall significantly (~30 %) below the linear scaling dependence of n_{ped} with I_p found over the B range 2.6-6.5 T, as shown in Figure 3. There is still a fairly narrow range of n_{ped} for given I_p and B_T, indicating that n_{ped} is largely determined by its target parameters. It should be noted that gas feedback is used to set the L-Mode target density and in most cases there is no external fuelling in H-mode. However, the 5-8 T data are better fit by an inverse dependence on q_{95}, as indicated

by the blue and red points in Figure 4. A q_{95}^{-1} dependence of ∇n would be consistent with particle diffusivity D_{eff} scaling with q_{95}[14]. However, lower B density pedestals lie systematically below such a scaling, as indicated by the green points (2.6-4 T) in Fig. 4. The density pedestal dependence is apparently more complex than previously suggested using data obtained in a narrower range of operating space.

While there is a range of pedestal pressures depending on the net power flux, the limiting pressure appears approximately independent of B_T for given I_p. This is despite the fact that most of these H-modes do not show evident large-scale MHD but are either EDA or ELM-free. The p_{ped} limit is consistent with a limiting $\alpha_{MHD} = 2\mu_o q^2 R p' / B^2$, which depends on I_p rather than B due to the q dependence. However, the lower n_e at higher B (higher q_{95}) shifts the balance between n_{ped} and T_{ped} towards higher temperature. This is illustrated in Figure 5, which compares discharges of matched shape, I_p=1.2 MA and input power 2.5 MW, at 5.4 and 7.85 T. The 7.85 T discharge has lower n_{ped} and 43% higher T_{ped}. Notably, the pressure profiles overlay closely. The similarity of p_{ped} implies, through profile stiffness, that global stored energy and confinement are also roughly independent of B at fixed I_p, which is found to be the case. Other high field discharges have T_{ped} up to 930 keV.

C. H-mode regimes and operation space

The higher T_{ped} and lower n_{ped} typical of high B discharges leads to significantly reduced ν^*_{ped}. Figure 6 shows the operational space of α_{MHD}, calculated at the pedestal midpoint assuming p_i=p_e, vs ν^* at the pedestal for 7.8-7.9 T discharges. We take Z_{eff}=1 in this computation since accurate edge ion and impurity data are not always available. ν^* is thus a lower bound; average Z_{eff} is typically between 1 and 2 in C-Mod. These are compared with a well characterized set of steady EDA discharges at 4.5-6 T, from a prior analysis of pressure pedestal scalings[13]. The high B discharges are at lower ν^* and/or lower α_{MHD} than the typical EDA operational space. Likely for this reason, most of these H-modes were transient in nature, with n_e and P_{rad} rising. Many (solid circles) were completely ELM-free. Some discharges at $q_{95} > 6$ had a quasi-coherent mode (open circles). However, its amplitude was apparently too weak to cause steady electron and impurity density. Previous studies have shown that the QC mode amplitude can vary

continuously between ELM-free (no QC) and steady EDA discharges, and is correlated with experimental D_{eff} [27]. The weak EDA discharges continue the trend of higher α_{MHD} with reduced ν^*, and extend the lower range of ν^*_{ped} for this regime to 0.44. Both of these trends enhance the regime's interest for burning plasma experiments. One discharge, at 1.3 MA (q_{95}=4.1) developed a few large, discrete ELMs with low baseline D_α, with ~10% drops in pedestal T_e.

III. Influence of field and current direction and magnetic configuration

A. Scrape-off-layer flows and plasma rotation

Motivated by the interesting results on SOL flows, threshold and rotation described in Section I, experiments were carried out to compare these parameters with different field directions. In typical C-Mod operation, referred to here as 'Normal B' or 'Forward B', B×∇B points downward to the closed lower divertor. Both field and current were reversed in direction in the 'Reversed B' case, keeping the same magnetic helicity but reversing B×∇B so that it pointed toward the top of the vacuum vessel. The Reversed B plasmas analyzed here had B_T =5.4 T and I_p = 800 kA, as for previous comparisons of different magnetic configurations[24]. As shown in Figure 7, the direction of parallel flows in the high-field-side SOL is *unaffected* by the change in field direction. In both cases the parallel Mach number, measured 2 mm outside the separatrix, is positive for lower single null (LSN) configurations (downward-pointing triangles) and negative for upper single null (USN). This is consistent with the flows being dominantly driven by transport fluxes which are largest at the outer midplane, and then flow along field lines to the active X-point[23]. Such flows should depend only on configuration, not field or current direction. However, because the direction of I_p as well as B_T was reversed, the parallel component of these flows is counter-I_p in Reversed B LSN, and co-I_p in Normal B LSN. Conversely, flows are counter-I_p in Normal B USN and co-I_p in Reversed B USN. In contrast to the inner SOL, parallel flows in the outer, low field side, SOL tend to be smaller and show a near-symmetrical change in sign as the direction of the magnetic field is reversed. This response is consistent with the dominant flow components in the outer SOL being a combination of co-current plasma rotation and Pfirsch-Schluter ion currents. These details, as well as some shifts in the operational space of SOL profiles, will be presented elsewhere. The essential result for threshold

experiments is that the flow directions in a physical frame of reference do not shift with field and current direction.

Core toroidal rotation in ohmic plasmas *does* change direction in the lab frame of reference, as shown by the top panel of Figure 8 which plots initial values of $V_{tor}(0)$ vs $\bar{n}_e$, before ICRF, for a number of LSN discharges. The sign convention is such that positive values are co-I_p in Normal B and counter-I_p in Reversed B. Ohmic rotation is counter- I_p current in both cases, consistent with intrinsic rotation being current-related[28]. However, the V_{tor} values vary; on average V_{tor} is more counter-current (~30 km/s) in Reversed B LSN as compared to Normal B (~-10 km/s). This is consistent with the counter-I_p SOL flows adding to the core rotation in Reversed B (unfavorable case), and co-I_p flows partially offsetting it in Normal B. The converse is true in USN plasmas, which are more strongly counter-current for Normal B (again the unfavorable case) than Reversed B.

B. L-H Thresholds and evolution of profiles and transport before the transition.

Figure 8 also shows the L-H total power thresholds for the same LSN plasma conditions (b). As expected, P_{LH} is significantly higher for the Reversed field (unfavorable) case, by a factor of 2 or more (2.7-3.7 MW, increasing weakly with density, compared to 1.1-1.7 MW for LSN). As shown in Fig. 8(c), edge T_e at the transition increases by an even greater factor. As found in prior studies, $T_{e,95}$ for Normal B LSN is ~100-200 eV; the discharges here were not controlled ramp discharges, and, as for the B_T comparison, the points represent simply the nearest preceding ETS measurement. In Reversed B and at midrange densities, $\bar{n}_e$ ~1.8- x10^{20} m^{-3}, $T_{e,95}$ at the L-H transition is ~400 eV, in approximate agreement with previous measurements in unfavorable drift direction[20,22]. Edge ∇T_e increases by a comparable fraction. More unexpected is the strong increase at lower n_e, below $\bar{n}_e$ =1.5 x10^{20} m^{-3}, with $T_{e,95}$ up to 770 eV. This behavior was not seen in a small number of prior Reversed B H-modes produced in 2000 at similar n_e, and H-modes in Normal B have been achieved at lower densities[29,20], with a minimum in P_{thresh} at about 0.9 x10^{20} m^{-3}. While the increase might suggest proximity to a low density limit, there is not a corresponding increase in the power threshold. $T_{e,95}$ values at high density ($\bar{n}_e$ > 2 x10^{20} m^{-3}) are lower, typically 300 eV, approaching those seen in Normal B. Transition temperature is

plotted vs P_{thresh}/n_e in Fig. 8(d). In contrast to the B_T scan of Fig. 2, there is a strong non-linearity indicating changing edge thermal transport as discussed below.

Edge profiles and rotation in Reversed B LSN typically evolve over several energy confinement times before reaching the L-H threshold conditions, particularly evident for the lower n_e cases. Figure 9 shows time traces for one such discharge, with ohmic target $\bar{n}_e = 1.1 \times 10^{20}$ m^{-3}. 3.4 MW of ICRH is turned on at 0.7 s, causing a gradual increase in $\bar{n}_e$ to 1.8×10^{20} m^{-3}; there is no apparent change in density gradient, or in D_α emission, until a clear L-H transition at 0.802 s. For comparison, τ_E is 30-40 ms during the L-mode phase. During this interval $V_{tor}(0)$ gradually decreases from 30 km/s (counter-I_p) to ~10 km/s. Edge T_e and T_i continuously increase, more rapidly starting at 0.772 s, when a break-in-slope is seen. Steep T_e gradients develop in the outer 2-3 mm of the plasma, with $\nabla P_e/n_e$ reaching -200 keV/m. Since P_{in} and n_e are constant, edge thermal transport must be decreasing during this period; an edge power balance for $0.97 \leq \psi \leq 1$ for this discharge shows χ_{eff} dropping from 0.4 m^2/s to 0.14 m^2/s. Unlike the later L-H transition, this change appears to be a slow, second-order change in transport. It is accompanied by gradual changes in broadband fluctuations, seen most clearly on magnetic coils near the outer midplane; magnetic fluctuations $\tilde{B}$ decrease in the 50-100 kHz band but increase at f > 150 kHz. The integral of $\tilde{B}$ over 5-250 kHz decreases by typically 45%. Stored energy also increases, with H rising to ~1.6 in L-mode, similar to observations of 'improved L-mode' on ASDEX Upgrade[22]. A more complete description and analysis of this slow change in confinement will be presented separately. It should be noted that this evolution in V_{tor} and edge T is also typically seen in Normal B USN plasmas[24,30], but has not been observed in favorable magnetic configuration, even when edge thresholds are comparably high as for example in 7.8 T H-modes.

The SOL flows, stronger ohmic counter-current rotation and subsequent decrease, higher power threshold, and higher edge T and ∇T with Reversed B as compared to Normal B LSN discharges are all consistent with prior results varying magnetic configuration at fixed B direction. In the 'unfavorable case', the SOL flows appear to increment the core rotation, and presumably conditions at the plasma edge, in such a way that ohmic conditions are further from the threshold

conditions for an H-mode transition. Higher input powers are then needed to counteract these unfavorable conditions and achieve the transition. If, as is widely held, a critical E_r shear is needed, the flows either modify the threshold condition, or lead to E_r components (through V_{pol} or V_{tor}) which counteract the larger diamagnetic term $\nabla P/n$ before a transport bifurcation occurs.

C. H-mode pedestals and regimes of operation

Following the L-H transition in particle confinement, H-mode pedestals in both temperature and density develop as usual in Reversed B LSN discharges. Edge χ_{eff} drops sharply, to 0.05 m^2/s in the discharge shown in Fig. 9, and fluctuations decrease markedly across all frequency bands. The widths, pressure gradients and confinement in fully developed H-modes are similar to those in Normal B H-modes of similar I and B. The most apparent difference is, as was the case for high field H-modes, in the pedestal T_e and n_e. Figure 10 compares n-T operational spaces for 5.4 T, 800 kA Reversed B H-modes, including many of the discharges from Fig. 8, with a set of 5.4 T H-modes, mainly at 900 kA, in the same shape but at Normal B. Time slices are at least 40 ms after an L-H transition to avoid transients, and again no external fuelling is used during the H-mode. The target density and power ranges for the two data sets were similar, $\bar{n}_e$ =1.3-2.7 x10^{20} m^{-3}, and $P_{RF} \leq 4.4$ MW. The bulk of the Reversed B H-modes are at higher T_{ped}, up to 900 eV, than the Normal B H-modes, which mainly have T_{ped} 200-550 eV. Pedestal densities in Reversed B are lower. These differences have a large effect on ν^*_{ped}, with most Reversed B pedestals at 0.33-2 (again assuming Z_{eff} =1). α_{MHD} ranges typically from 6 to 13, higher than is usual at this field. Comparing with Figure 6, it is seen that the normalized operational space of 5.4 T Reversed B H-modes is more closely aligned with the 7.9 T Normal B pedestals than those at 5.4 T, an unexpected result. Likely related to this, and again similar to the 7.9 T case, most Reversed B H-modes tended to be rather transient in nature, as opposed to the steady EDA typical of Normal B 5.4 T H-modes. Some of the Reversed B LSN H-mode plasmas had weak QC modes, indicating the presence of EDA and providing the opportunity to measure the propagation direction of the mode in this configuration. Previous measurements have shown that the QC mode propagates with $\mathbf{k}\cdot\mathbf{B}$ approximately 0 in the electron diamagnetic drift (poloidal projection), counter-I_p direction (toroidal projection)[31]. In the reversed B, reversed I_p LSN

configuration the QC mode propagation also reversed, remaining in the electron diamagnetic/counter-I_p direction. This observation rules out hypotheses that its direction is set by edge flows or x-point configuration.

IV. Discussion and Conclusions

The C-Mod experiments reported here have extended studies of the H-mode formation and pedestal to new operational parameters, in particular to higher field, and to unfavorable magnetic configuration with respect to the B×∇B drift. Both of these aspects are challenging experimentally in that the H-mode power threshold is, as expected, high; P_{thresh} was typically > 3 MW in both cases, close to the power routinely available (~3-4.5 MW) at the time of these experiments. This tends to constrain the range of target density for which H-modes can be obtained, since P_{thresh} rises at both high and low $\bar{n}_e$. Another common feature was that the edge temperatures, and ∇T, were significantly higher than in more typical 5.4 T, favorable configuration cases. $T_{e,95}$ was often >400 eV at the L-H transition, a value typical of H-mode pedestals in low B, high n_e EDA H-modes. It is perhaps not surprising, then, that T_{ped} in fully developed H-modes was also high, in the range ~400-800 eV. The higher T_{ped} in the unfavorable configuration, with the same target plasma parameters, is particularly suggestive in this regard. Past studies varying target density at near-constant threshold T_e have shown that this affects the balance between n_e and T_e in the evolving H-mode, with lower n_e L-modes giving lower n_{ped} and higher T_{ped}[27]; apparently a similar effect results from changing L-mode T_e. This implies a need to consider threshold and pedestal scaling physics in a more unified manner than is typically done.

Pedestal widths do not show systematic variation over the wide ranges of I_p and B_T explored here, or with magnetic configuration. Pressure gradients are also, to first order, constant for given I_p. $p_{e,ped}$ is thus essentially constant with B, or configuration. Through profile stiffness, which holds in all these conditions, core confinement and stored energy are also unchanged. The high field, and reversed field, discharges with higher T_{ped} thus also tended to have lower n_{ped}; it is difficult to be certain of the causality in this relation. Because $\nu^* \sim n/T^2$, even small shifts in the

n-T balance significantly reduce ν^*_{ped}, which has been extended to lower values than in typical C-Mod H-modes. QC modes in EDA tend to be weaker and H-modes more transient. On the positive side, the trend of higher α_{MHD} at lower ν^* has continued, giving the prospect of higher pedestal pressures; the limits in this space have likely not yet been reached. Increasing B of course allows for higher I_p and therefore p_{ped}, though the upper ranges have not yet been explored on C-Mod at maximum power. The results in this initial study motivate further high field H-mode experiments at higher P_{RF}, up to the 5-6 MW ICRH achieved during other campaigns[32], which should further expand the accessible pressure range and perhaps density range, potentially enabling study of the high β 'small ELM' regime and likely extending p_{ped} and W to higher values.

Pedestal density at high B falls below the previously observed linear scaling with I_p. Probably more important than the empirical scaling remains the fact that n_{ped} is difficult to vary following H-mode formation, responding very weakly to gas fuelling when barriers are strong and the SOL is opaque to neutrals. This is compounded when P_{thresh} is high and close to the maximum available power, leaving less scope either for varying the target density, or for strong puffing which tends to cool the edge and can cause an H-L back-transition. ITER is expected to also have P/P_{thresh} near one as well as an opaque SOL, indicating that scenarios for forming and fuelling H-modes to the desired target need to be carefully considered. ITER will likely be similarly difficult to fuel with gas[33], so that pellet fuelling is required. How this affects the H-mode parameters requires further study.

Experiments with reversed B and I_p, with fixed configuration, have provided important information on the variation of the L-H threshold. In particular, the invariance of high field side SOL flows with B direction is consistent with an origin in particle fluxes driven by radial transport localized to the low field side. These flows are near-symmetric between USN and LSN, confirming that differences in top and bottom divertor geometry are not the major influence. As noted, flows and profiles in the outer (LFS) SOL do show differences between favorable and unfavorable drift direction. The more counter-I_p core rotation with unfavorable

drifts is consistent with an offset induced by SOL flows, and with the higher L-H power threshold, though the origin and scaling of this rotation remains complex and poorly understood. Also unclear is the physical mechanism by which the L-H threshold is affected by flows and rotation, e.g. by changing the threshold criterion or the net E_r profiles at the edge. The observation of slowly evolving T_e pedestals in the unfavorable case, before the clear L-H transition in particle confinement, is relevant to this. Strong T_e and p_e gradients build up in "L-mode". This slow, apparently second order, transition contrasts with prior observations of the L-H bifurcation[34,35].

While the basic 'improved L-mode' phenomenology has been reported elsewhere[22], it has not been explained. The new observations of gradually changing fluctuations appear important in this regard. Further analysis of fluctuations, flows and E_r, and comparison with turbulence models is planned. Slow transitions in DIII-D with an X-point near the divertor floor, dubbed the 'Intermediate Mode', had several global features in common with this phenomenon, but were characterized by periodic bursts of fluctuations and flux not seen here[36]. While the primary interest in this regime is for transport physics, it may also be of interest as a target for advanced scenarios since it has good confinement ($H_{ITER89\text{-}P} \leq 1.6$) but low density which is advantageous for external current drive. The fact that a modest change in χ_e over a 2 mm region in the plasma edge can cause a >50% increase in global confinement underscores the continuing importance of understanding this critical and complex region of the plasma.

ACKNOWLEDGEMENTS

The authors wish to acknowledge the efforts of the entire Alcator C-Mod team, in particular the RF group, in carrying out the experiments reported here. This work was supported by U.S. Dept. of Energy Contract Nos. DE-FC02-99ER54512 and DE-FG03-97-ER54415.

Figures

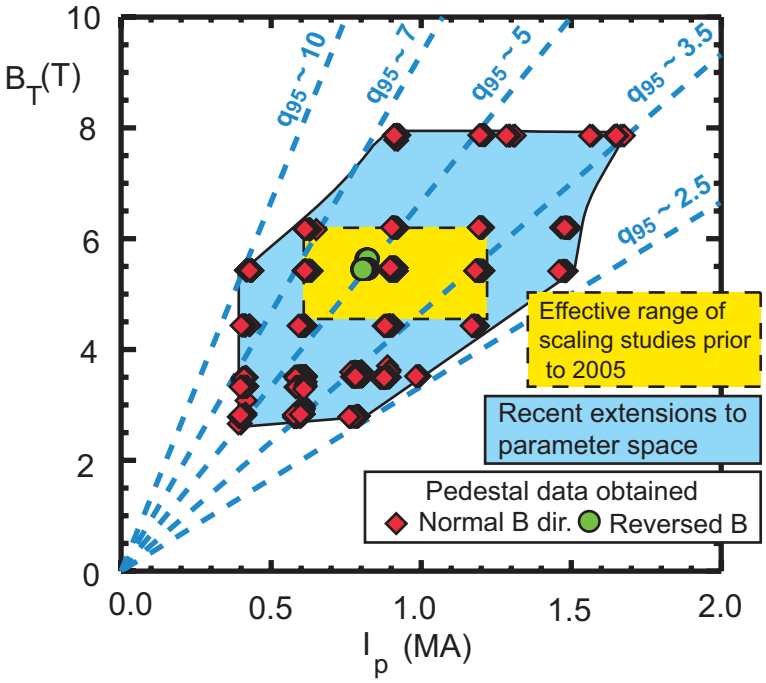

Figure 1: Operational space in B_T vs I_p for pedestal scaling studies reported in this paper, mainly with 'Normal B_T' (diamonds). For comparison, the smaller dashed rectangle indicates the parameters studied prior to 2005. Circles indicate the parameters of 'Reversed B_T' discharges.

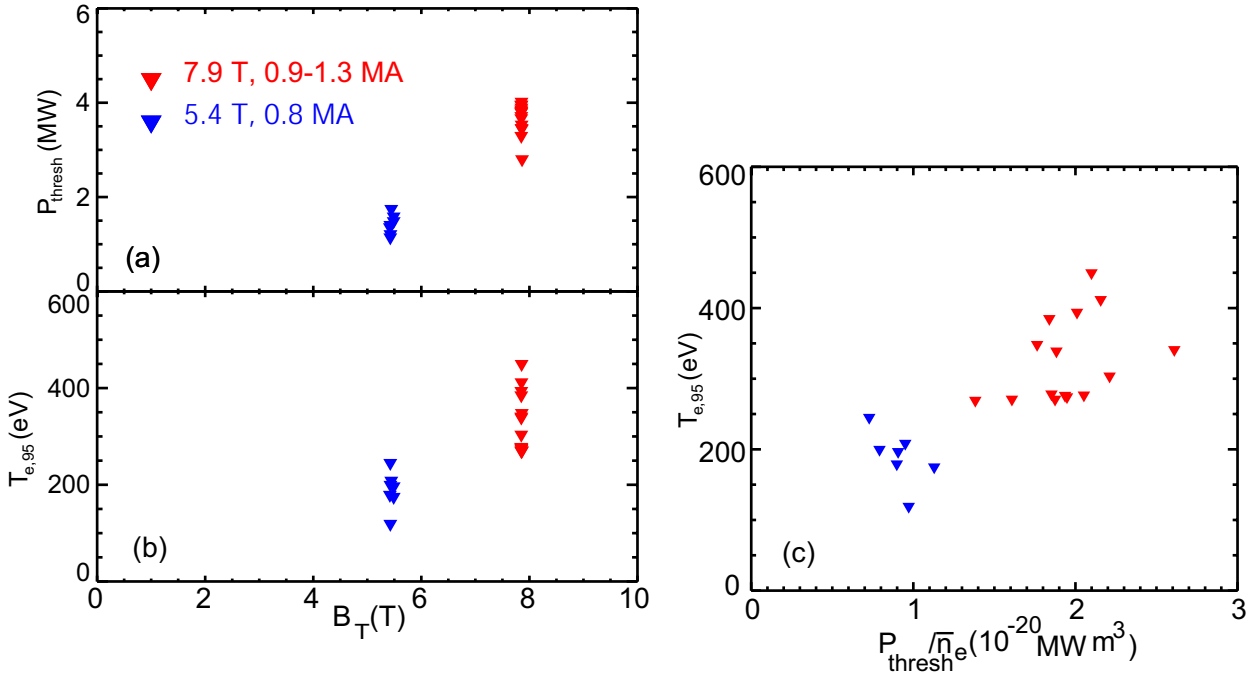

Figure 2: Total power P_{thresh} at the L-H transition (a) and T_e at the 95% poloidal flux surface (b) vs B_T for a set of C-Mod discharges. (c) $T_{e,95}$ vs P_{thresh}/n_e for the same dataset.

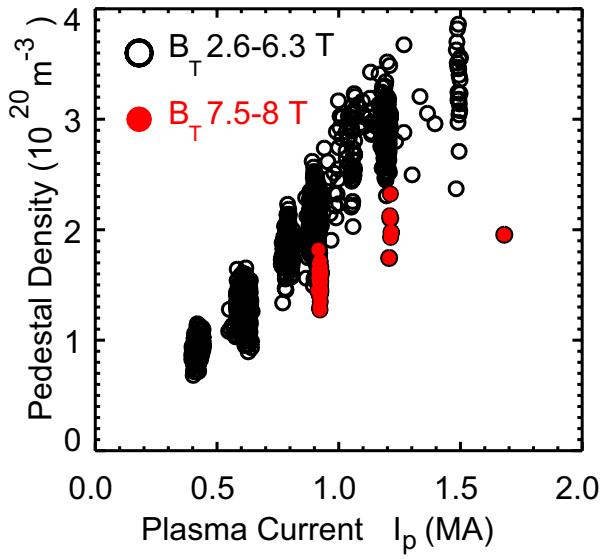

Figure 3: Pedestal density vs I_p for a set of H-mode discharges with near-constant shape, and no external fuelling or pumping during the H-mode. Pedestals at 2.6-6.3 T (open circles) scale approximately linearly with I_p as shown in Ref. 14, while higher B H-modes (7.5-8 T, closed red points) fall below this scaling. q_{95} ranges from 2.6 to 9.5.

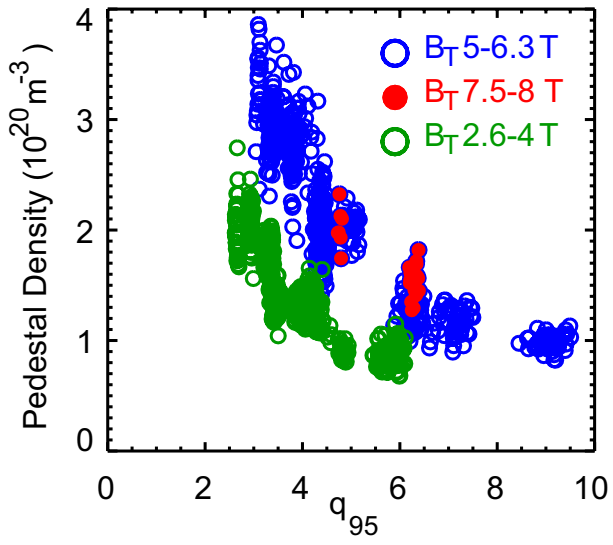

Figure 4: (Color online). Pedestal density vs q_{95} from the same set of H-mode discharges as Fig 3. Pedestals at 5-8 T (blue, red points) scale inversely with q_{95}, while lower B H-modes (green) fall below this scaling.

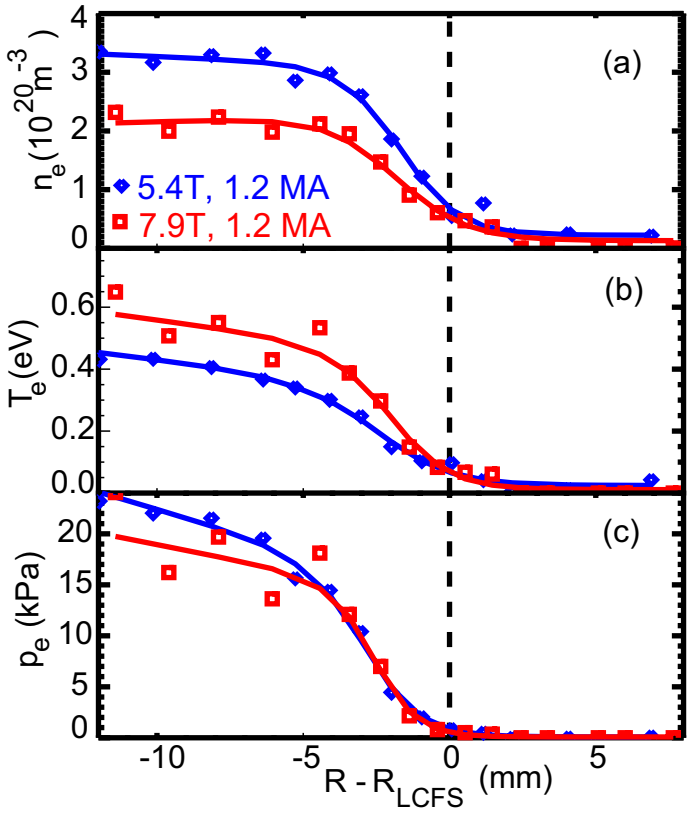

Figure 5: Comparison of electron pedestal profiles for 1.2 MA discharges at 5.4 T (shot 1050624022, blue diamonds) and 7.85 T (shot 1060426015, red squares). Both discharges had 2.5 MW ICRF. Note that pedestal pressures (c) overlay well, but that the higher B discharge has lower n_{ped} (a) and higher T_{ped} (b); this is reflected in the full datasets in these conditions.

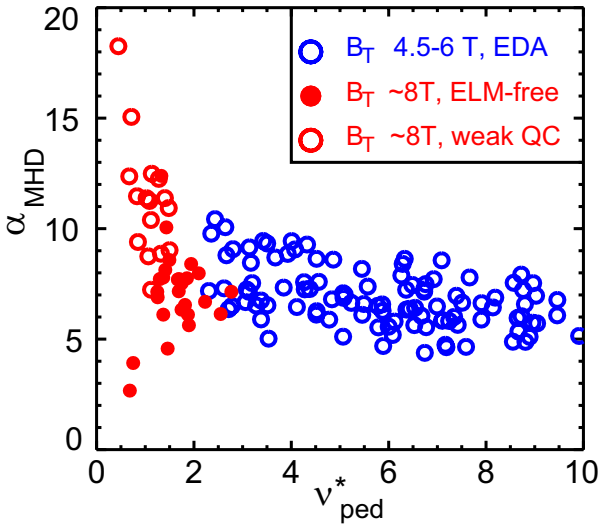

Figure 6: (Color online). Normalized pressure gradient α_{MHD} vs ν^*_{ped}, defined as in the text, for a set of 7.85 T discharges (red points) with P_{RF}=1.2-4.8 MW RF, I_p= 0.9-1.7 MA, $\bar{n}_e$ =1.3-2.2x10^{20}m^{-3}. These H-modes were typically evolving in time and points represent single time slices; times within 20 ms of a transition are excluded. These are compared with dataset of steady EDA H-modes (blue points) at 4.5-6 T from Ref. 13. Solid points are ELM-free, while open red points had a quasicoherent mode, though not steady n_e.

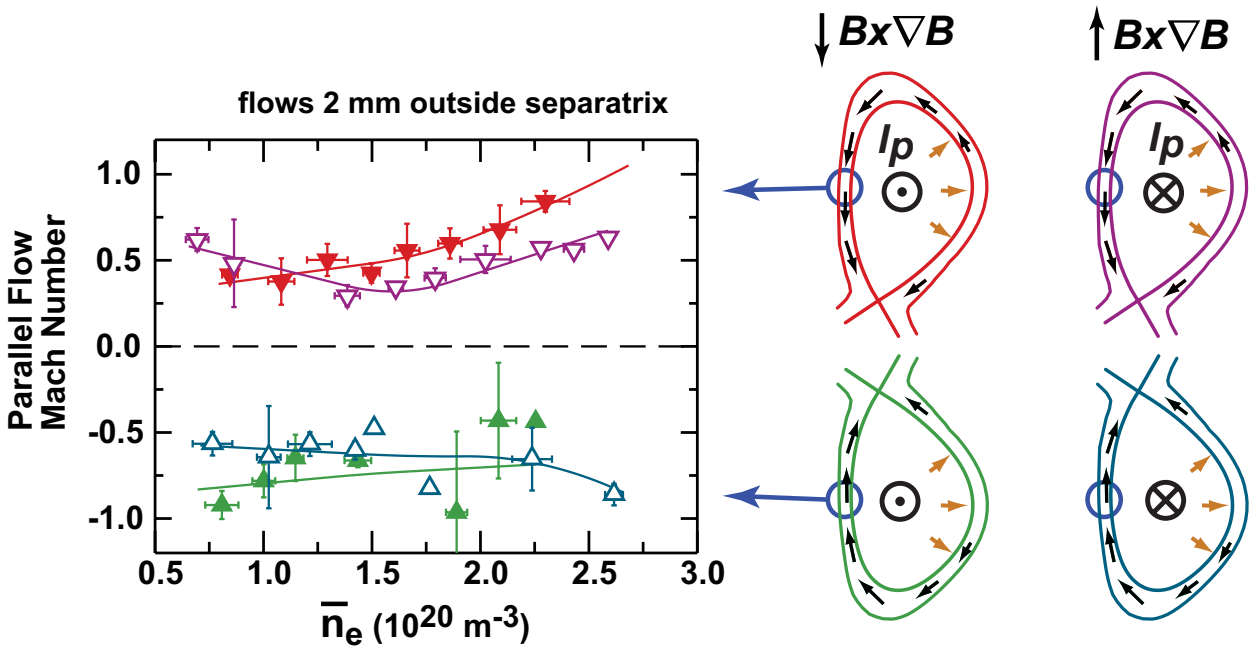

Figure 7: Mach number of parallel flows measured in the High Field Side SOL, 2mm outside the separatrix, vs $\bar{n}_e$ for LSN (downward triangles) and USN (upward triangles). Closed symbols represent normal field and current directions and open symbols reversed B and I_p. Flows are positive with LSN and negative with USN, and of similar magnitude independent of B, I direction.

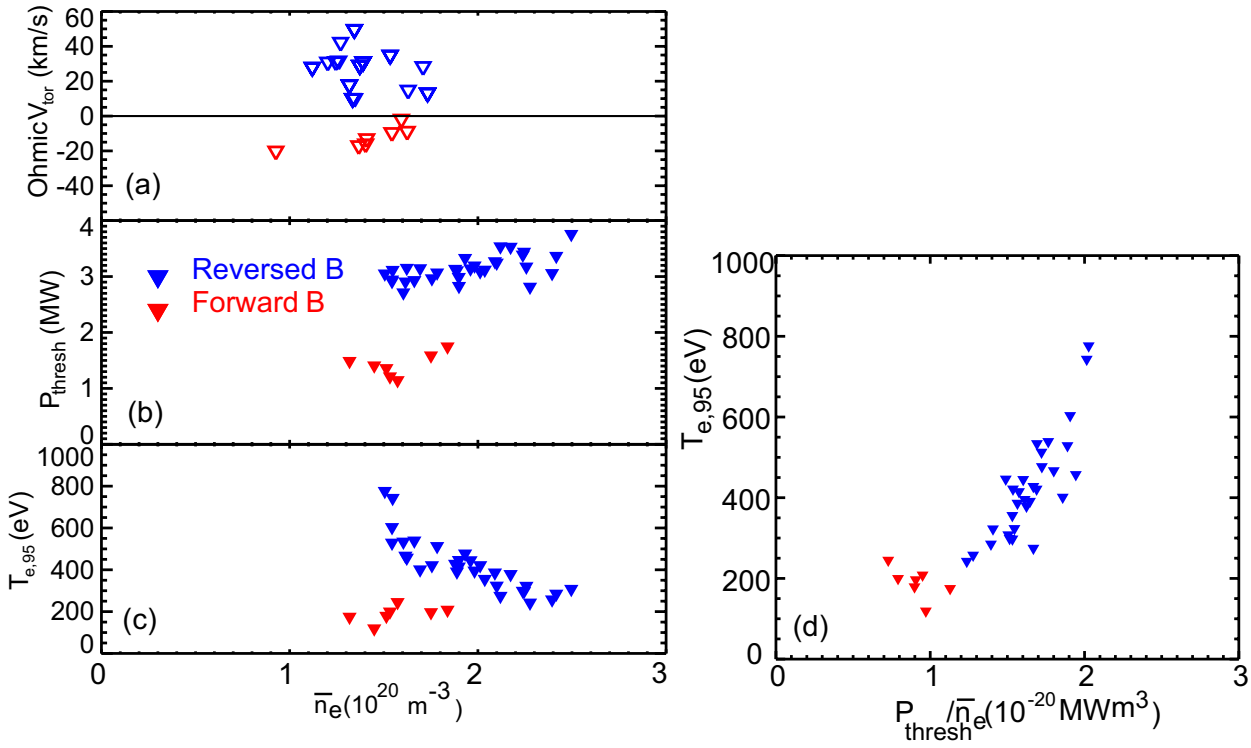

Figure 8: Variation of rotation and L-H threshold with B direction for LSN plasmas. Red points are normal (favorable) direction, and blue are reversed I and B. (a) Core V_{tor} vs $\bar{n}_e$ for the ohmic target plasma, in lab frame; positive velocity is co-I_p for normal B and counter-I_p for reversed B. Rotation is counter-I_p in each case, but larger on average in the unfavorable case. (b) L-H power threshold vs $\bar{n}_e$ at the transition, higher in reversed B. $T_{e,95}$ at the transition (c) is also much higher, particularly near the low n_e limit. (d) T_e vs P_{thresh}/n_e for the same dataset, showing non-linearity at high values.

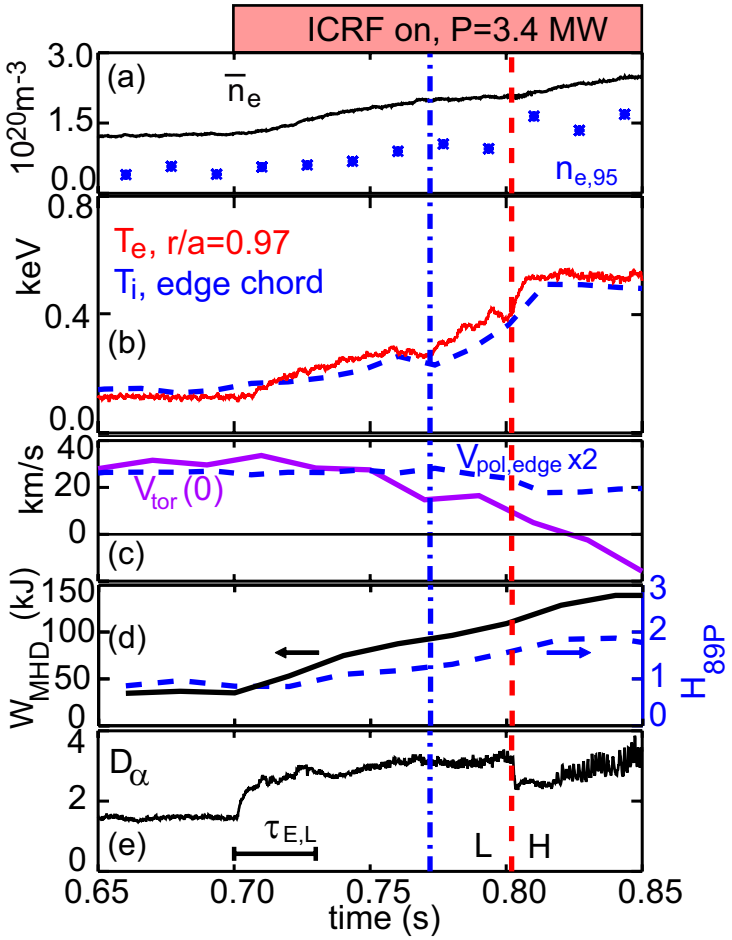

Figure 9: Time evolution in L-mode in a 5.4 T, 0.8 MA reversed B LSN discharge. 3.4 MW of ICRF is turned on at 0.7 MW. (a) Average (solid line) and edge ($n_{e,95}$, *) density increase initially due to outgassing, but no barrier develops until the L-H transition seen on D_α at 0.082 s (e). (b). Edge T_e (solid) and T_i (dashed) increase continuously, more rapidly from 0.772 s. (c) Core V_{tor} (solid) continuously decreases, while edge V_{pol} (dashed, multiplied by 2 for clarity)) decreases slightly at the T_e break-in-slope, and further at the L-H transition. (d) Stored energy W_{MHD} (solid, left axis) and normalized confinement time $H_{ITER89-P}$ (dashed, right axis) also increase.

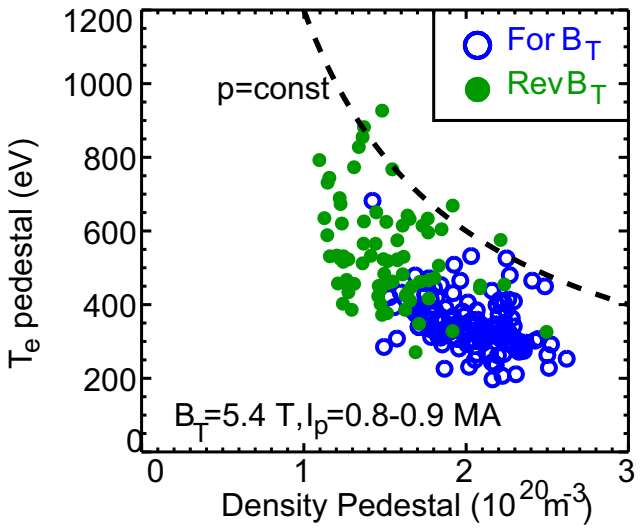

Figure 10: (Color online). Operational space of pedestal T_e vs n_e for sets of 5.4 LSN discharges with Forward B (open blue points) and Reversed B (closed green points). Points represent single time slices at least 40 ms from an L-H transition.

REFERENCES:

[1] I. H. Hutchinson, R. Boivin, F. Bombarda *et al*, Phys. Plasmas **1**, 1511 (1994).

[2] F. Wagner, G. Fussman, T. Grave *et al*, Phys. Rev. Letters **53**(11), 1453-1456 (1984).

[3] M Greenwald, R. L.Boivin, F. Bombarda *et al*, Nucl. Fusion **37** (6), 793-807 (1997).

[4] W. Suttrop, M. Kaufmann, H. J. de Blank *et al*, Plasma Phys. Control. Fusion **39** 2051-2066 (1997).

[5] J. A Snipes, R. S. Granetz, M. Greenwald *et al*, Nuclear Fusion **34** 1039 (1994).

[6] J. W. Hughes, A. E. Hubbard, D. Mossessian, *et al*, *H-mode Pedestal and L-H Transition Studies*, to be published in Fusion Science and Technology.

[7] Y. Takase, R. Boivin, F. Bombarda *et el*, Phys. Plasma*s* **4** (5), 1647 (1997).

[8] D. A. Mossessian, P. Snyder, M. Greenwald, J. W. Hughes, Y. Lin, A. Mazurenko, S. Medvedev, H.R. Wilson and S. Wolfe, Plasma Phys. Contr. Fusion **44** (4), 423-437 (2002).

[9] N. Oyama, P. Gohil, L.D. Horton *et al* Plasma Phys. Control. Fusion **48**, 5A, A171-181 (2006).

[10] A. E. Hubbard, K. Kamiya, N. Oyama, N. Basse, T. Biewer, E. Edlund, J.W. Hughes, L. Lin, M. Porkolab, W. Rowan, J. Snipes, J. Terry and S.M. Wolfe, Plasma Phys. Controlled Fusion **48**, 5A, A121 (2006).

[11] J. L. Terry, I. Cziegler, A.E. Hubbard, J.A. Snipes, J.W. Hughes, M.J. Greenwald, B. LaBombard, Y.Lin, P. Phillips, and S. Wukitch, *The dynamics and structure of edge localized modes in Alcator C-Mod*, to be published in J. Nucl. Materials (2007).

[12] J. W. Hughes, D. A. Mossessian, A. E. Hubbard, E. S. Marmar, D. Johnson and D. Simon, Rev. Sci. Instr. **72**(1) 1107-1110 (2001).

[13] J. W. Hughes, D. A. Mossessian, A. E. Hubbard, B. LaBombard and E. S. Marmar, Phys. Plasmas **9**(7), 3019 (2002).

[14] J. W. Hughes, B. LaBombard, D. A. Mossessian, A. E. Hubbard, J. Terry, T. Biewer and the Alcator C-Mod team, Physics of Plasmas **13**, 056103 (2006).

[15] A. E. Hubbard, Plasma Phys. Contr. Fusion **42** (5A), A15-A36 (2000).

[16] R. J. Groebner, M. A. Mahdavi, A. W. Leonard, T. H. Osborne, N. S. Wolf, G. D. Porter, P. C. Stangeby, N. S. Brooks, R. J. Colchin and L. W. Owen, Nucl. Fusion **44** 203 (2004).

[17] B. LaBombard, J. W. Hughes, D. Mossessian, M. Greenwald, B. Lipschultz, J. L. Terry and the Alcator C-Mod team, Nucl. Fusion **45** 1658 (2005).

[18] J. W. Hughes, B. LaBombard and J. Terry, 33rd EPS Conference on Plasma Phys. Rome, 19 - 23 June 2006, Europhysics Conference Abstracts Vol. 30I, P5.133 (2006).

[19] J. W. Hughes, B. LaBombard, J. Terry, A. Hubbard and B. Lipschultz, *Edge Profile Stiffness and Insensitivity of the Density Pedestal to Neutral Fueling in Alcator C-Mod Edge Transport Barriers*, Paper EX/P3-9, to be published in Proc. 21st IAEA Fusion Energy Conference, Chengdu, China, Oct. 2006.

[20] A. E. Hubbard, R. L. Boivin, J. F. Drake, M. Greenwald, Y. In, J. H. Irby, B. N. Rogers and J. A. Snipes, Plasma Phys. Control. Fusion **40**, 689-692 (1998).

[21] R. J. Groebner and T. N. Carlstrom, Plasma Phys. Control. Fusion **40**, 673-677 (1998).

[22] F. Ryter, W. Suttrop, B. Brusehaber *et al*, Plasma Phys. Control. Fusion **40**, 725-729 (1998).

[23] B. LaBombard, J. E. Rice, A. E. Hubbard, J. W. Hughes, M. Greenwald, J. H. Irby, Y. Lin, B. Lipschultz, E. S. Marmar, C. S. Pitcher, N. Smick, S. M. Wolfe, S. J. Wukitch and the Alcator Group, Nucl. Fusion **44** 1047 (2004).

[24] B. LaBombard, J. E. Rice, A. E. Hubbard, J. W. Hughes, M. Greenwald, R. S. Granetz, J. H. Irby, Y. Lin, B. Lipschultz, E. S. Marmar, K. Marr, D. Mossessian, R. Parker, N. Smick, J. A. Snipes, J. L. Terry, S. M. Wolfe and the Alcator C-Mod Team, Phys. Plasmas **12** 056111 (2005).

[25] J. E. Rice, W. D. Lee, E. S. Marmar *et al*, Phys. Plasmas **11** (5) 2427-2431 (2004).

[26] J. A. Snipes and the International H-mode Threshold Database Working Group, Plasma Phys. Control. Fusion **42**, A299-A308 (2000).

[27] A. E. Hubbard, R. Boivin, R. S. Granetz *et al*, Phys. Plasmas **8**(5) 2033 (2001).

[28] J. E. Rice, W. D. Lee, E. S. Marmar, P. T. Bonoli, R. S. Granetz, M. J. Greenwald, A. E. Hubbard, I. H. Hutchinson, J. H. Irby, Y. Lin, D. Mossessian, J. A. Snipes, S. M. Wolfe and S. J. Wukitch, Nuclear Fusion **44** 379-386 (2004).

[29] F. Ryter and the H-Mode database working group, Nuclear Fusion **36**(9), 1217 (1996).

[30] J. E. Rice, A. E. Hubbard, J. W. Hughes, M. J. Greenwald, B. LaBombard, J. H. Irby, Y. Lin, E. S. Marmar, D. Mossessian, S. M. Wolfe and S. J. Wukitch, Nuclear Fusion **45** 251-257 (2005).

[31] J. L. Terry, N. P. Basse, I. Cziegler *et al*, Nucl. Fusion **45** (11) 1321-1327 (2005).

[32] B. Lipschultz, Y. Lin, M. L. Reinke, A. Hubbard, I. H. Hutchinson, J. Irby, B. LaBombard, E.S. Marmar, K. Marr, J. L. Terry, S. M. Wolfe and the Alcator C-Mod group, Phys. Plasmas **14** 056117 (2006).

[33] A. S. Kukushkin, H. D. Pacher, G. W. Pacher, G. Janeschitz, D. Coster, A. Loarte and D. Reiter, Nucl. Fusion **43** 716 (2003).

[34] A. E. Hubbard, B. A. Carreras, N. P. Basse, D. del-Castillo-Negrete, J. W. Hughes, A. Lynn, E. S. Marmar, D. Mossessian, P. Phillips and S. Wukitch, Phys. Control. Fusion **46**, A95 (2004).

[35] A. E. Hubbard, B. A. Carreras, R. L. Boivin, J. W. Hughes, E. S. Marmar, D. Mossessian and S. J. Wukitch, Phys. Control. Fusion **44**, A359 (2002).

[36] R. J. Colchin, M. J. Shaffer, B. A. Carreras *et al*, Phys. Rev. Lett. **88** (25), 255002-1 (2002).